Int. J. Electrochem. Sci., 14 **(2019)** 11379 – 11390, doi: 10.20964/2019.12.70

International Journal of
ELECTROCHEMICAL
SCIENCE
www.electrochemsci.org

Oxygen evolution electrocatalytic properties of perovskite-type $La_{1-x}Sr_xCoO_3$ ($0 \leq x \leq 0.8$) oxides obtained by polyvinylpyrrolidone sol-gel route

Narendra Kumar Singh[*], *Priya Sharma, Indresh Kumar and Amritpal Singh Chaddha*

Department of Chemistry, Faculty of Science, University of Lucknow, Lucknow-226007, India
[*]E-mail: nksbhu@yahoo.com, singh_narendra@lkouniv.ac.in,

Received: 25 July 2019 / *Accepted:* 24 August 2019 / *Published:* 29 October 2019

Perovskite-type oxides of La, Sr and Co have been prepared via a sol-gel route using nitrate salt of metals and polyvinylpyrrolidone (PVP40) as precursors. The electrocatalytic properties of the material was investigated by recording cyclic voltammogram (CV) and anodic polarization curve in 1 M KOH at 25 ^oC. The experiments have been performed in a three-electrode single compartment glass cell in which the synthesized oxide was taken as anode in the form of film electrode. Auxiliary and reference electrodes were Pt-foil (area ~ 2 cm^2) and Hg/HgO/1M KOH, respectively. The CV recorded in the potential region 0.0 – 0.7 V, exhibited an anodic (Ep_a = 495±14 mV) and corresponding cathodic peaks (Ep_c = 353 ± 38 mV) prior to onset of oxygen evolution reaction (OER). Anodic polarization study indicates that substitution of Sr in the base oxide ($LaCoO_3$) enhanced the electrocatalytic properties of the material. The activity was found to be highest with 0.8 Sr-substitution. At E = 800 mV, it produced current density j = 261.8 mA cm^{-2}, which is about 65 times higher than the base oxide. Values of Tafel slope and reaction order as given in Table 2, describe that each oxide electrode has different mechanistic path towards OER. Thermodynamic parameters, such as standard entropy of activation ($\Delta S^{\circ\#}$), standard enthalpy of activation ($\Delta H^{\circ\#}$) and standard electrochemical energy of activation ($\Delta H_{el}^{\circ\#}$) have been estimated for each oxide electrode. Materials have also been analysed for their perovskite phase and morphology by using X-ray diffraction (XRD) and scanning electron microscope (SEM) techniques, respectively.

Keywords: Perovskite-type oxide, PVP method, XRD, Oxygen evolution, Electrocatalytic activity, Thermodynamic parameters

1. INTRODUCTION

Perovskite-type oxides of La with Ni, Co, Fe, Mn and their metal- substituted products are known to be efficient electrocatalysts having wide range of applications such as an electrode material for alkaline fuel cell [1,2], water electrolysis and fuel cell [3-7], as heterogeneous catalysts for oxidation of

unburnt hydrocarbon and CO, reduction of NO exhaust [8-10] and as low cost cathode or anode for O_2 reduction [11] or O_2 evolution [12], respectively. Oxide materials obtained by higher temperature methods [13-18] have large particle size, low specific surface area and therefore low electrocatalytic properties.

During last few decades, investigations have been made and some low temperature synthetic routes [19-23] have been developed to produce oxides with low particle size and high specific surface area. These methods generally require precursors of amorphous organic acids, like malic acid (MA), citric acid (CA), polyacrylic acid (PAA), citric acid-ethylene diamine (CA-EDA) etc, which facilitate to give the homogeneity in the metal ions and thereby produce the material relatively at lower temperature. By adopting these methods and some other methods, such as spray pyrolysis (spray), sequential solution coating (SSC), hydroxide solid solution (HSS) and precipitation, Singh et al. [24-37] synthesized $LaCoO_3$, $LaMnO_3$, $LaNiO_3$ and their metal-substituted derivatives and used them as anode for alkaline water electrolysis. They found that the electrocatalytic power of oxides, obtained by low temperature methods, was much better than those prepared by conventional ceramic [38, 39] and high temperature thermal decomposition [13] methods. Recently, we developed Sr [40] and Cu-substituted [41] lanthanum cobaltate by using citric acid-ethylene glycol (CA-EG) and malic acid sol-gel route, respectively and studied their electrocatalytic properties towards OER. During recent years, some Fe-based perovskite oxides have been reported [42, 43] for their oxygen evolution electrocatalytic properties in alkaline medium. Sarkar et al. [42] produced $La_{1-x}Ca_xFe_{3-\delta}$ by combustion method and found maximum activity with x = 1.0 mol towards OER. The BSCF perovskite oxides [43] obtained by glycine-nitrate auto-combustion method have been used as bifunctional electrocatalysts with oxygen evolution current density 10 mA cm^{-2} at E = 1.65 V vs RHE. Júlio C. Sczancoski et al. [44] studied OER on Fe-doped $LaNiO_3$ deposited on pyrolytic graphite sheets and found the highest electrocatalytic activity for $LaNi_{0.4}Fe_{0.6}O_3$ with Tafel slope value of 52 mV $decade^{-1}$. The findings of above research articles and literature revealed that the electrocatalytic properties of oxides strongly affected by preparation method, precursors used in the synthesis, metal ion substitution, pH of the solution and preparation temperature.

In this paper, we used a new precursor, polyvinylpyrrolidone (PVP) having mol. wt. 40000, for the synthesis of Sr-substituted lanthanum cobaltate and studied their electrocatalytic properties with regards to OER. Polyvinylpyrrolidone is a water-soluble polymeric material and has excellent emulsifying and wetting properties. These properties enable metal ions for the easy nucleation and produce oxide material at low temperature. Results of the study, so obtained, are described in this paper.

2. EXPERIMENTAL

Materials, $La_{1-x}Sr_xCoO_3$ ($0 \leq X \leq 0.8$), were prepared by adopting the method reported elsewhere [45]. According to this, aqueous solution of $La(NO_3)_3.6H_2O$ (Himedia, 99.0%), $Co(NO_3)_3.6H_2O$ (Merck, 98%), $Sr(NO_3)_2$ (Merck, 99.0%) and was prepared in stoichiometric ratio. To this, polyvinylpyrrolidone (Sigma-Aldrich, Molecular Wt. 40,000) with ratio, PVP: 3 times the total moles of cations, was added. A gel like mass was obtained on evaporation of the solution with constant stirring. The gel further decomposed at higher temperature to get the precursors of perovskite-oxide. The polymerized precursors

were then heat treated at 600 ºC for 6h in a PID controlled electrical furnace (ASCO, India) in and get the desired products.

The perovskite phase of the synthesized materials was confirmed by recording the X-ray diffraction. For the purpose, XPERT-PRO Diffractometer (Model PW3050/60) having radiation Source Cu-Kα (λ = 1.54048 Å) was used. Scherrer's formula was used to calculate the crystallite size of the materials. The texture of the oxide in the form of powder was examined by scanning electron microscope (JOEL JSM 6490LV).

The electrocatalytic properties of the synthesized oxides have been performed in the form of film electrodes. For the purpose, slurry was prepared by mixing the oxide powder with few drops of Triton X-100 (Merck, 98.0%). This slurry was then coated to one side of the pre-treated Ni plate (area = 1.5 cm^2) with the help of fine brush and subsequently heat treated at 380 °C for 1½ hr. For desired loading of the oxide powder on the substrate, coating process was repeated 2-3 times. The oxide film was then converted into electrode by making the connection with copper wire, silver paste and Araldite epoxy. The cleaning of Ni-support and formation of oxide film electrode were performed in the similar way as mentioned in the literature [24, 29]. An electrochemical workstation (Gamry Reference 600 ZRA) provided with potentiostat/galvanostat and corrosion & physical electrochemistry software was used to run the cyclic voltammogram (CV) and anodic polarization experiments. The equipment is connected to the desktop computer (HP) where all the data were recorded and stored. During the experiment, a platinum foil (~2 cm^2), Hg/HgO/1M KOH (E° = 0.098 V vs NHE at 25°C) and oxide film electrode were used as auxiliary, reference electrode and working electrode, respectively. The was the oxide film electrode. In order to make the proper connection between working and reference electrode and to minimize the ohmic resistance (iR drop), Luggin capillary (agar-agar and potassium chloride gel) was employed in the electrochemical cell.

The electrochemical order of reaction was determined by recording the anodic polarization curve in different KOH (Merck, 98.0%) concentration at 25 °C. During the experiment, ionic strength (μ = 1.5) was kept constant by using inert electrolyte KNO_3 (Merck, 98.0%). The standard electrochemical energy of activation and other thermodynamic parameters have been calculated from the polarization curve recorded in 1M KOH at different temperatures.

3. RESULT AND DISCUSSION

3.1 Physicochemical Properties

3.1.1 Scanning Electron Micrograph (SEM)

SE-micrographs of $LaCoO_3$ and its Sr-substituted products were taken in the form of powder and shown in the Fig. 1 (a-d) at magnification ×500. Figure shows that the Sr-substitution in the base oxide strongly affected the texture of the material. Flakes like structure has been observed in the micrograph, but the size of the flakes was found to decrease with the substitution of Sr for La in the base oxide.

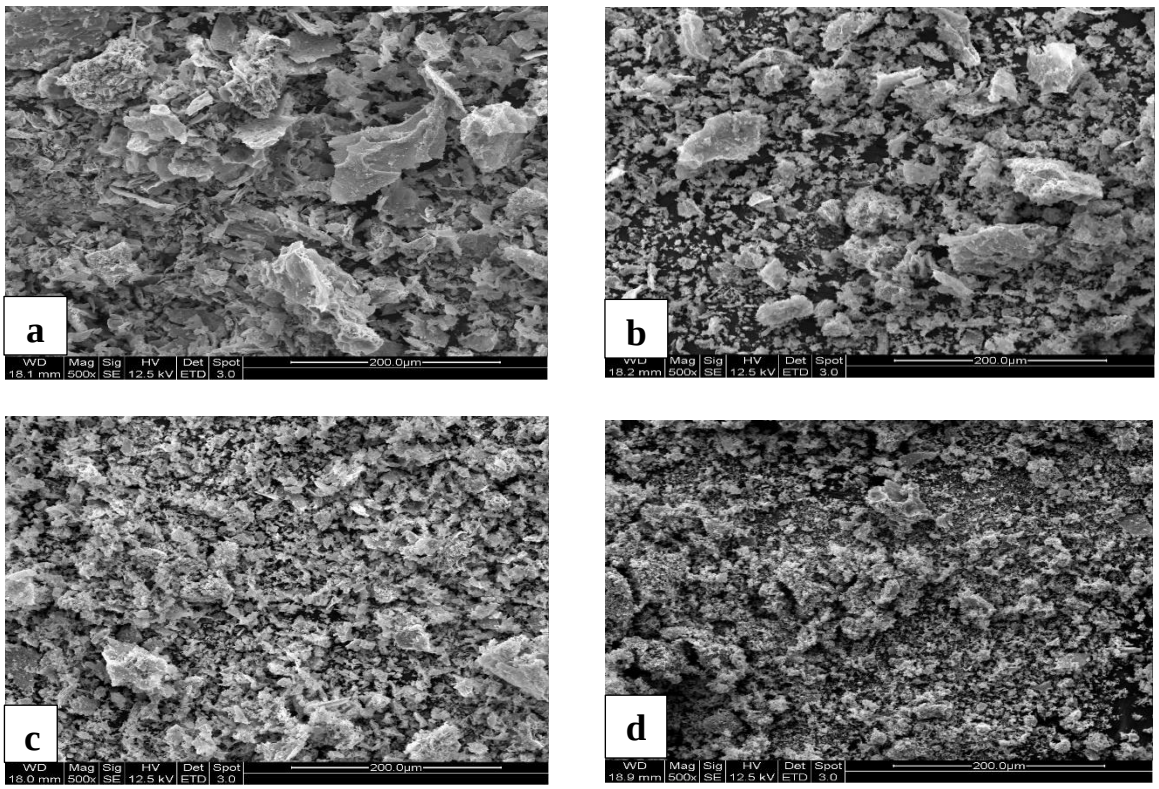

Figure 1. SE Micrographs of oxide powder sintered at 600 ˚C for 5 h. a: $LaCoO_3$, b: $La_{0.8}Sr_{0.2}CoO_3$, c: $La_{0.4}Sr_{0.6}CoO_3$, d: $La_{0.2}Sr_{0.8}CoO_3$

3.1.2 X-ray diffraction (XRD)

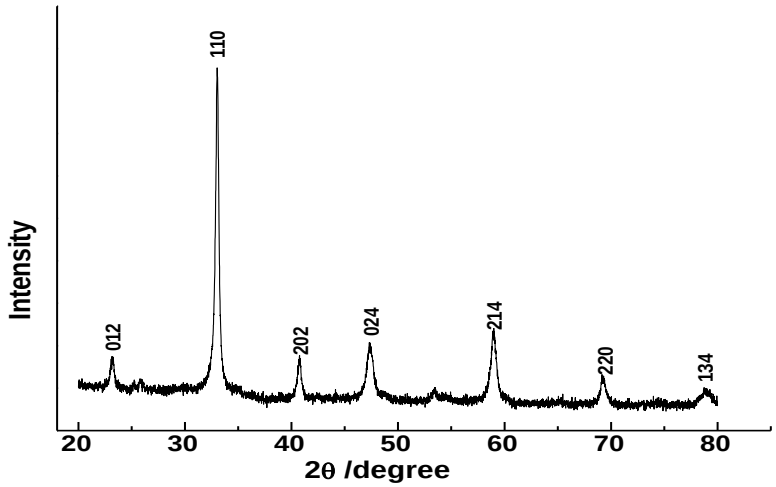

Figure 2. X-ray diffraction patterns of $La_{0.2}Sr_{0.8}CoO_3$ sintered at 600 ˚C for 5 h;

Fig. 2 represents the X-ray diffraction pattern of $La_{0.2}Sr_{0.8}Co_3$, sintered at 600 ºC for 5h in 2θ = 20° to 80°. Values of 2θ and 'd' corresponding to each diffraction lines were found to be very close to their respective JCPDS ASTM file 25-1060 and followed hexagonal crystal geometry. The observed data of the diffraction pattern indicates that the PVP method produced the material with almost pure

perovskite phase. Scherer's formula [46], $S = 0.9\lambda/B\cos\theta$, was used to calculate the crystallite size of the material and found to be ~ 18 nm for $La_{0.2}Sr_{0.8}Co_3$ oxide. In the Scherer equation, λ is the wavelength of radiation, B is the full width at half of the most intense peak and θ is the corresponding angle.

3.2. Electrochemical properties

3.2.1. Cyclic Voltammetry (CV)

Redox behaviour of each oxide film electrodes on Ni was determined by recording cyclic voltammogram between 0.0 - 0.7 V potential region in 1 M KOH at 25 °C (scan rate = 20 $mVsec^{-1}$). In order to avoid any complexity, CV curve of only three composition is shown in Fig. 3.

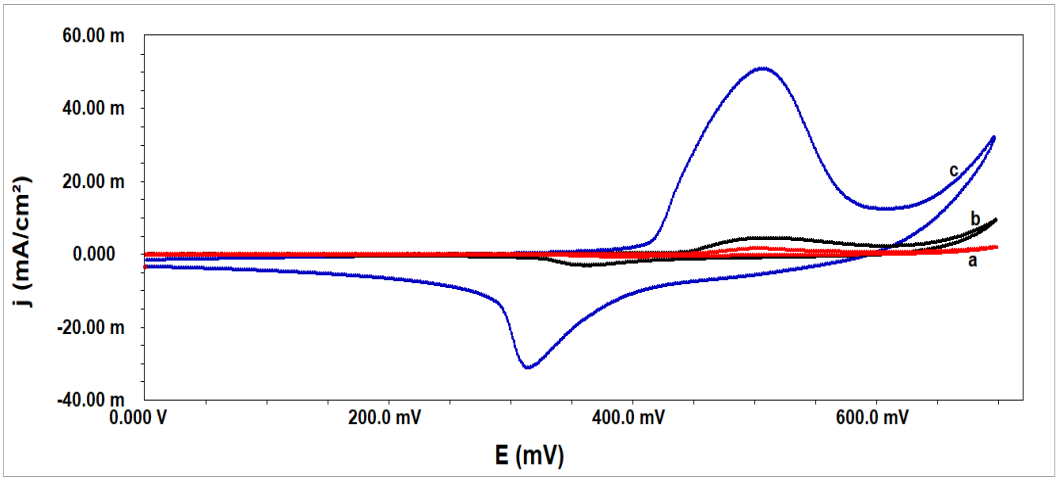

Figure 3. Cyclic voltammograms of Ni/ $La_{1-x}Sr_xCoO_3$ ($0 \leq x \leq 0.8$) in 1M KOH at 25˚C; (scan rate = 20 mV sec^{-1}) a: $La_{0.8}Sr_{0.2}CoO_3$, b: $La_{0.4}Sr_{0.6}CoO_3$, c: $La_{0.2}Sr_{0.8}CoO_3$

Table 1. Values of the cyclic voltammetric parameters of Ni/ $La_{1-x}Sr_xCoO_3$ ($0 \leq X \leq 0.8$) in 1 M KOH at 25 °C (scan rate = 20 mV sec^{-1}).

Electrode	E_{Pa} /mV	E_{Pc} /mV	ΔE_p /mV	E° /mV	j_{pa}	j_{pc}	j_{pa}/j_{pc}
$LaCoO_3$	482	372	110	427	1.2	0.4	2.6
$La_{0.8}Sr_{0.2}CoO_3$	503	391	112	447	1.6	0.7	2.3
$La_{0.4}Sr_{0.6}CoO_3$	509	361	148	435	4.5	3.1	1.5
$La_{0.2}Sr_{0.8}CoO_3$	505	315	190	409	50.9	31.0	1.6

Each voltammogram was observed to be similar to that reported in literature [24, 29, 47] and has a pair of redox peaks, an anodic (Ep_a = 495 ± 14 mV) and corresponding cathodic (Ep_c = 353 ± 38 mV), prior to the oxygen evolution reaction. Values of peak potentials (E_{Pa} & E_{Pc}), peak separation potential ($\Delta E_P = E_{Pa} - E_{Pc}$) and formal redox potential {$E° = (E_{Pa}+E_{Pc})/2$} were estimated from the CV curve and are listed in Table 1. The value of redox peaks obtained with each oxide electrode was found to be very

similar to that for bare Ni [48]. This indicates that the redox peaks might be originated due to contact of electrolyte with Ni substrate during the cycle process. Also, it has been reported [3, 49] that oxides prepared at low temperature undergo hydration easily in electrolytic solution. As a result of this the electrolyte may penetrate the oxide film and come in contact with the Ni-substrate through pores, cracks and grain boundaries.

The effect of scan rate on the redox behaviour has also been studied in 1M KOH at 25°C. A representative cyclic voltammogram for Ni/$LaCoO_3$ at different scan rates is shown in the Fig. 4. The nature of CV curve obtained at different scan rates is almost similar to that observed at scan rate of 20 mV sec^{-1}. The only difference is that as we increase the scan rates from 20 to 120 mV sec^{-1} the anodic and cathodic peaks shifted towards higher and lower potential sides, respectively. The observed shifting in the peaks indicates the quasi-reversible nature of the redox couple. The anodic and cathodic peak currents also observed to vary with scan rates. From table 2, it is found that the ratio of anodic and cathodic peak current is more than unity, which indicates the irreversible nature of the redox process.

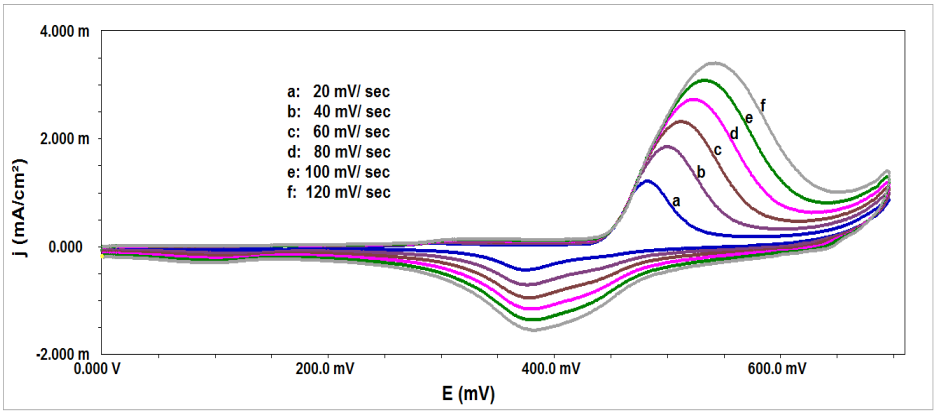

Figure 4. Cyclic voltammogram of the Ni/$LaCoO_3$ film electrode at different scan rates in 1M KOH (25˚C)

3.2.2. Electrocatalytic activity

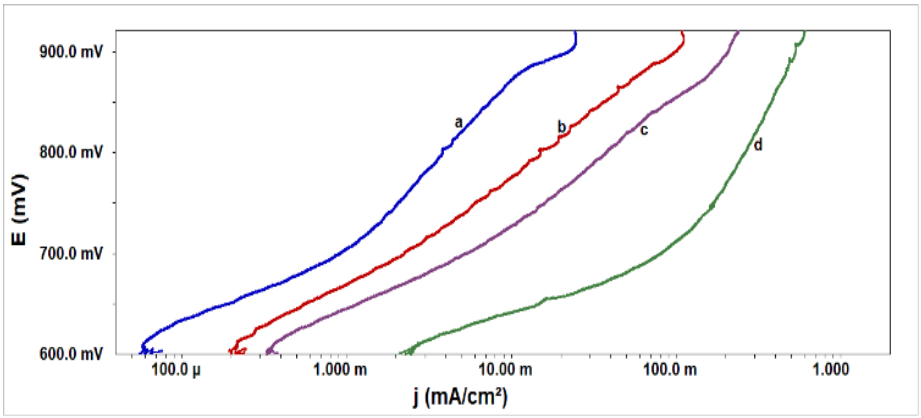

Figure 5. Tafel plots for oxygen evolution on Ni/$La_{1-x}Sr_xCoO_3$ ($0 \leq x \leq 0.8$) in 1M KOH at 25 ˚C; scan rate: 0.2 mVsec^{-1} a: $LaCoO_3$, b: $La_{0.8}Sr_{0.2}CoO_3$ c: $La_{0.4}Sr_{0.6}CoO_3$, d: $La_{0.2}Sr_{0.8}CoO_3$

The electrocatalytic activity of each oxide electrocatalyst was determined by recording jR-compensated anodic polarization curves (E vs.log j) at a slow scan rate of 0.2mV sec^{-1} in 1M KOH at 25 °C. The observed polarization curve is shown in Fig. 5.

The electrocatalytic activity in terms of potential at constant current density as well as in terms of current density at constant potential and Tafel slope were estimated from the polarization curve. Values, so obtained, are given Table 2. Table 2 indicates that the Tafel slope value was found to minimum (52 mV $decade^{-1}$) with most active, $La_{0.2}Sr_{0.8}CoO_3$, electrode and values of other electrodes lied between 52 and 86 mV $decade^{-1}$. The substitution Sr for La strongly affected the electrocatalytic activity of the material. On the comparison of electrocatalytic activity in terms of current density at fixed potential of 800 mV, it was found that 0.8 mol Sr-substituted oxide has about 67 time more current density than the base oxide ($LaCoO_3$).

Based on the current density data at constant potential (E = 800 mV), the electrocatalytic activity of different oxide electrodes show the following order:

$La_{0.2}Sr_{0.8}CoO_3$ (j = 261.8 $mAcm^{-2}$) > $La_{0.4}Sr_{0.6}CoO_3$ (j = 37.6 $mAcm^{-2}$) > $La_{0.8}Sr_{0.2}CoO_3$ (j = 15.1 $mAcm^{-2}$) > $LaCoO_3$ (j = 3.9 $mAcm^{-2}$)

Table 2. Electrode kinetic parameters for oxygen evolution reaction on $La_{1-x}Sr_xCoO_3$ ($0 \leq x \leq 0.8$) electrodes in 1 M KOH at 25°C

Electrode	Tafel slope (b) (mV/decade)	Order (p)	E / mV at j (mA cm^{-2})		j (mA cm^{-2}) at E / mV	
			10	100	700	800
$LaCoO_3$	69	~2.3	874	1110	0.9	3.9
$La_{0.8}Sr_{0.2}CoO_3$	86	~1.4	776	902	2.2	15.1
$La_{0.4}Sr_{0.6}CoO_3$	71	~1.2	728	857	5.4	37.6
$La_{0.2}Sr_{0.8}CoO_3$	52	~1.2	642	711	81.8	261.8

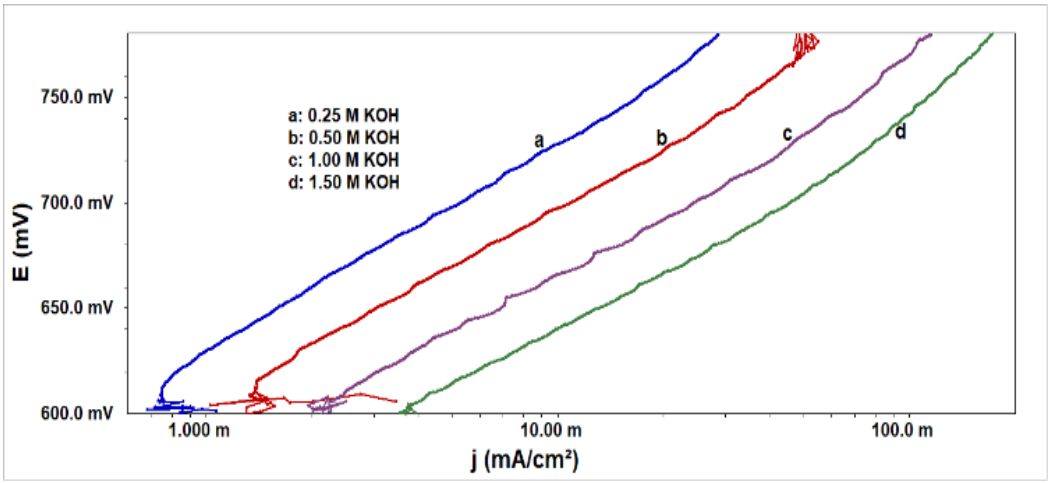

Figure 6. Tafel plots for oxygen evolution on Ni/$La_{0.2}Sr_{0.8}CoO_3$ at varying KOH concentrations (μ = 1.5) at 25 ˚C.

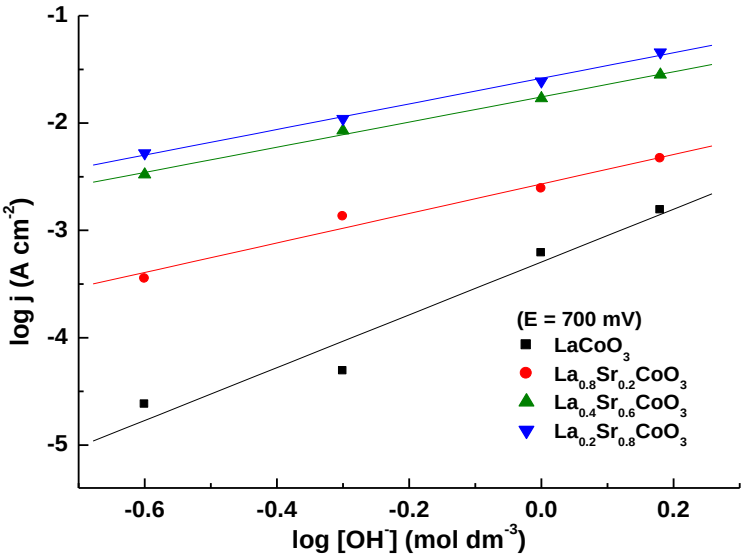

Figure 7. Plot of log j vs log [OH^-] for Ni/$La_{1-x}Sr_xCoO_3$ ($0 \leq x \leq 0.8$) electrodes at 700 mV

The order of oxygen evolution reaction with each oxide electrode was determined by recording the anodic polarization curve in different KOH concentrations at 25 °C. In order to maintain the electrical intensity uniform, the ionic strength of each solution was kept constant. The polarization curve of electrocatalysts in varying KOH concentrations was observed to similar. A representative curve for Ni/$La_{0.2}Sr_{0.8}CoO_3$ is shown in the Fig. 6.

Table 3. Comparison with reported perovskite-type oxides for oxygen evolution reaction

Electrocatalysts	Electrolyte	Tafel Slope (mV/decade)	E /mV (vs Hg/HgO) at j = 100 mA cm^{-2}	Preparation method	Ref.
$La_{0.7}Sr_{0.3}CoO_3$	1 M KOH	70	677	PAA sol-gel	[29]
$La_{0.8}Sr_{0.2}MnO_3$	1 M KOH	108	816	MA sol-gel	[31]
$La_{0.6}Sr_{0.4}MnO_3$	1 M KOH	108	822	CA sol-gel	[32]
$La_{0.6}Sr_{0.4}MnO_3$	1 M KOH	103	828	PAA sol-gel	[33]
$La_{0.7}Sr_{0.3}MnO_3$	1 M KOH	92	780	CA-EDA sol-gel	[36]
$La_{0.7}Sr_{0.3}CoO_3$	1M KOH	64	671	Precipitation method	[37]
$La_{0.2}Sr_{0.8}CoO_3$	1M KOH	70	686	CA sol-gel	[40]
$La_{0.6}Cu_{0.4}CoO_3$	1 M KOH	90	734	MA sol-gel	[41]
$La_{0.7}Sr_{0.3}MnO_3$	1 M LiOH	---	~2 mA cm^{-2} at 750 mV	Auto combustion	[53]
$La_{0.2}Sr_{0.8}MnO_3$	6 M KOH	---	152 mA cm^{-2} at 700 mV	Sol-gel method	[54]
$La_{0.2}Sr_{0.8}CoO_3$	**1 M KOH**	**52**	**711**	**PVP sol-gel**	**Present work**

From the polarization curve, the current density (in A cm^{-2}) data was collected at a certain potential. A plot log j vs. log [OH^-], as shown in the Fig. 7, was constructed for each oxide electrode at a constant potential of E = 700 mV. The slope of straight line, so obtained, determines the order of reaction and values are given in Table 2. The fractional order of reaction obtained with each electrocatalyst is very common and it has already been reported in literature [50-52]. The observed values of Tafel slope and reaction order as given in Table 2 suggest that the OER taking place at the electrocatalysts follows different mechanistic path. The electrocatalytic activity of the most active oxide electrode, $La_{0.2}Sr_{0.8}CoO_3$, of the present study has been compared with perovskite oxides obtained by other methods and data summarized are shown in Table 3. On comparison at current density of 100 mA cm^{-2}, the oxide prepared by PVP sol-gel route produced lower potential over most of the oxides. Only oxides obtained by PAA, CA sol-gel and precipitation methods showed better electrocatalytic activity than PVP sol-gel method. Also, the Tafel slope value was found to be lowest with the oxide electrode of present study.

3.2.3. Thermodynamic Parameters

The effect of temperature on OER has also been studied with each oxide electrodes in 1M KOH. A set four polarization curves at 20, 30, 40, and 50 °C obtained with $La_{0.2}Sr_{0.8}CoO_3$ is shown in Fig. 8. During the experiment, the temperature of the reference electrode was kept constant.

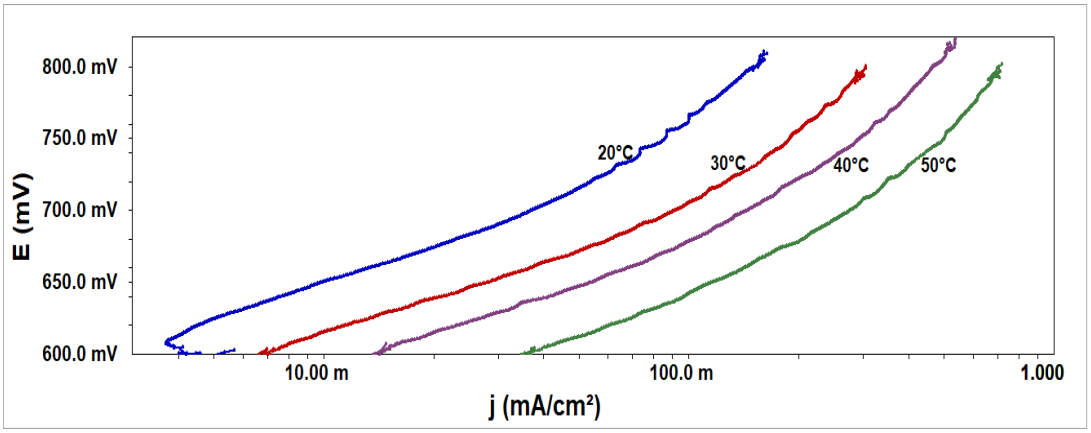

Figure 8. Tafel plots for the $La_{0.2}Sr_{0.8}CoO_3$ film electrode on Ni at different temperatures in 1 M KOH, a: 20 ˚C, b: 30 ˚C, c: 40 ˚C, d: 50 ˚C

The standard apparent enthalpy of activation ($\Delta H_{el}^{\circ\#}$) was estimated from the slope of Arrhenius plot, log j vs 1/T (Fig. 9), constructed at a certain potential (E = 650 mV).

The standard enthalpy of activation ($\Delta H^{\circ\#}$) and standard entropy of activation ($\Delta S^{\circ\#}$) were calculated by using following relations (1) and (2) [55], respectively,

$$\Delta H_{el}^{\circ\#} = \Delta H^{\circ\#} - \alpha F\eta \quad \ldots. (1)$$

$$\Delta S^{\circ\#} = 2.3R\,[\log j + \Delta H_{el}^{\circ\#}/2.3RT - \log (nF\omega C_{OH^-})] \quad \ldots(2)$$

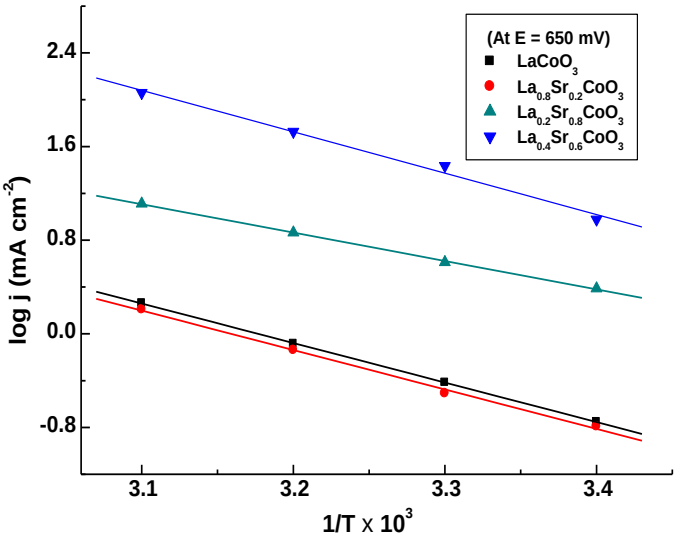

Figure 9. The Arrhenius plot at a constant applied potential (650 mV) for $La_{1-x}Sr_xCoO_3$ ($0 \leq x \leq 0.8$) in 1 M KOH

In equation (1), α (= 2.303RT/bF) is the transfer coefficient, where R, F and T are the gas constant, Faraday constant and absolute temperature, respectively. 'b' is the Tafel slope (in mV decade^{-1}) determined from the polarization curve recorded at different temperature. The overpotential (η) is determined by the relation $\eta = E - E_{O2/OH^-}$, where E and E_{O2/OH^-} (= 0.303 V vs. Hg/HgO) are the applied potential [56] across the catalyst/ 1 M KOH interface and the theoretical equilibrium Nernst potential in 1 M KOH at 25 ˚C, respectively. In equation (2), all the terms have their usual meaning. The frequency term ω (= k_BT/h) where, k_B and h are the Boltamann constant and Plank's constant, respectively. Estimated values of all the thermodynamic parameters are given in the Table 3. As expected, the $\Delta H_{el}^{\circ\#}$ value was found to be minimum (46.5$^{\#}$ kJ mol^{-1}) with most active electrode, $La_{0.2}Sr_{0.8}CoO_3$. However, for other electrodes, value of $\Delta H_{el}^{\circ\#}$ was observed to similar. The value of $\Delta S^{\circ\#}$ was found to highly negative which suggests the adsorption phenomena in the oxygen evolution reaction.

Table 4. Thermodynamic parameters for O_2 evolution on $Ni/La_{1-x}Sr_xCoO_3$ ($0 \leq x \leq 0.8$) in 1 M KOH.

Electrode	$\Delta H_{el}^{\circ\#}$ (kJ mol^{-1}) at E = 650 mV	$-\Delta S^{\circ\#}$ (Jdeg^{-1} mol^{-1})	α	$\Delta H^{\circ\#}$ (kJ mol^{-1})
$LaCoO_3$	65.0	139.1	0.8	91.8
$La_{0.8}Sr_{0.2}CoO_3$	65.0	140.2	0.7	88.5
$La_{0.4}Sr_{0.6}CoO_3$	66.4	111.7	0.7	89.8
$La_{0.2}Sr_{0.8}CoO_3$	46.5	168.3	0.6	66.6

4. CONCLUSION

In this paper, we have demonstrated the electrocatalytic properties of Sr-substituted lanthanum cobaltate in alkaline solution. The XRD data revealed the formation of almost pure perovskite phase of

the material with hexagonal crystal geometry. Substitution of Sr for La strongly affected the texture as well as electrocatalytic activity of the oxides. At E = 800 mV, the oxide, $La_{0.2}Sr_{0.8}CoO_3$, produced current density j = 261.8 mA cm^{-2}, while $LaCoO_3$ produced only j = 3.9 mA cm^{-2}. So, the electrocatalytic activity of $La_{0.2}Sr_{0.8}CoO_3$ is about 65 times higher than the base oxide. The activation energy value and morphology also authenticated the better electrocatalytic property of 0.8 mol Sr-substituted oxide.

ACKNOWLEDGEMENTS
Authors are thankful to Department of Chemistry, Lucknow University, Lucknow for providing basic infrastructure and BSIP, Lucknow for SEM analyses. One of the author N. K. Singh is thankful to Department of Science and Technology (DST), New Delhi for electrochemical work station under Fast Track Scheme for Young Scientist (No.: SR/FT/CS–044/2009).

References

1. D. B. Meadowcroft, *Nature*, 226 (1970) 847.
2. Y. Shimizu, K. Uemura, H. Matsuda, N. Miura, Y. N. Yamazoe, *J. Electrochem. Soc.*, 137 (1990) 3430.
3. S. Trasatti, in *The Electrochemistry of Novel Materials*, ed. J. Lipkowaski and Philip N. Ross, VCH Weinheim, 1994, p. 207.
4. E. J. M. O'Sullivan, E. J. Calvo, In *Electrode Kinetic Reaction*, ed. R. G. Compton, Elsecier, Amsterdam, 1987.
5. S. Trasatti, G. Lodhi., In *Electrodes of Conductive Metallic Oxides*, Part B, ed. S. Trasatti, Elsevier, Amsterdam, 1981.
6. L.G. Tejuca, J. L. F. Feierro, J. M. Tascon, *Advances in Catalysis*, Vol. 36, Academic Press, New York, 1991.
7. A. K. Ladovos and P. Pomonis, J. *Chem. Soc. Faraday Trans*., 87 (1991) 3291.
8. T. Ishihara, Y. Tsuruoka, T. Todaka, H. Nishiguchi, Y. Takita, *Solid State Ionics*, 152 (2002) 709.
9. T. Ishihara, M. Ando, K. Sada, K. Takiishi, K. Yamada, H. Nishiguchi, Y. Takita, *J. Catal.*, 220 (2003) 104.
10. R. J. H. Voorhoeve, D. W. Johnson, J. P. Remeika, P. K. Gollagher, *Science*, 195 (1977) 827.
11. Y. Matsumoto, H. Yoneyama, H. Tamura, *J. Electroanal. Chem*., 83 (1977) 237.
12. Y. Matsumoto, E. Sato, *Nippon Kagaku Kaishi*, (1981) 1709.
13. J. O. M. Bockris and T. Otagawa, *J. Electrochem. Soc*., 131 (1984) 290.
14. J. Balej, *Int. J. Hydrogen Energy*, 10 (1985) 89.
15. A. G.C. Kobussen, F. R. van Buren, T. G. M van Den Belt and H. J. A van Wees, *J. Electroanal Chem*., 96 (1979) 123.
16. Y. Matsumotp, H. Manabe, E. Sato, *J. Electrochem Soc*. 123 (1980) 811.
17. H. Wendt, V. Plzak, *Electrochim Acta*, 28 (183) 27.
18. G. Fiori, C. M. Mari, *Int. J. Hydrogen Energy*, 7 (1982) 489.
19. Y. Terayoka, H. kakebayashi, I. Moriguchi, S. Kagawa, *Chem. Lett*., (1991) 637.
20. K. Vidyasagar, J. Gopalkrishanan, C. N. R. Rao, J. *Solid State Chem*., 58 (1985) 29.
21. H. Taguchi, D. Matsuda, M. Nagao, *J. Am. Ceram. Soc*., 76 (1992) 201.
22. S. P. Sharibaa, P. J. Pomonis, A. J. Sdoukos, *J. Mater. Chem*., 1 (1991) 781.
23. J. K. Vassiliou, M. Hornbostel, R. Ziebarth, F. J. Disalvo, *J. Solid State Chemistry*, 81 (1989) 208.
24. S. K. Tiwari, P. Chartier, R. N. Singh, *J. Electrochem. Soc*., 142 (1995) 148.

25. A. N. Jain, S. K. Tiwari, R. N. Singh and P. Chartier, *J. Chem. Soc. Faraday Trans*., 91 (1995) 1871.
26. R. N. Singh, A. N. Jain, S. K. Tiwari, G. Poillerat, P. Chartier, *J. Appl. Electrochem*., 25 (1995) 1133.
27. R. N. Singh, S. K. Tiwari, S. P. Singh, A. N. Jain, N. K. Singh, *Int. J. Hydrogen Energy*, 22 (1997) 557.
28. S. K. Tiwari, J. F Koenig, G. Poillerat, P. Chartier, R. N. Singh, *J. Appl. Electrochem*., 28 (1998) 114.
29. R. N. Singh, S. K. Tiwari, S. P. Singh, N. K. Singh, G. Poillerat, P. Chartier, *J. Chem. Soc. Faraday Trans*. 92 (1996) 2593.
30. A. N. Jain, S. K. Tiwari, R. N. Singh, *Ind. J. Chem*., 37A (1998) 125.
31. N. K. Singh, S.K. Tiwari, R. N. Singh, *Int. J. hydrogen Energy*, 23 (1998) 775.
32. T. Sharma, N. K. Singh, S.K. Tiwari, R. N. Singh, *Ind. J. Eng. Mat. Sci*., 5 (1998) 38.
33. N. K. Singh, B. Lal, R. N. Singh, *Int. J. hydrogen Energy*, 27 (2002) 885.
34. R. N. Singh, S. K. Tiwari, T. Sharma, P. Chartier, J. F. Koenig, *J. New Mat. Electrochem. Syst*., 2(1999) 65.
35. B. Lal, M. K. Raghunanda, M. Gupta, R. N. Singh, *Int. J. Hydrogen Energy*, 30 (2005) 723.
36. B. Lal, N. K. Singh &, R. N. Singh, *Ind. J. Chem*., 40 A (2001), 1269.
37. R. N. Singh & B. Lal, *Int. J. Hydrogen Energy*, 27 (2002) 45.
38. Y. Matsumoto, H. Manabe & E. Sato, *J. Electrochem. Soc*., 127 (1980) 811.
39. Y. Matsumoto, S. Yamada, T. Nashida & E. Sato, *J. Electrochem. Soc*., 127 (1980) 2360.
40. M. K. Yadav, Ritu Yadav, Priya Sharma, N. K. Singh, *Int. J. Electrochem. Sci*., 11 (2016) 8633.
41. N. K. Singh, M. K. Yadav & Carlos Fernandez, *Int. J. Electrochem Sci*., 12 (2017) 7128.
42. Ravi Sankannavar & A. Sarkar, *Int. J. Hydrogen Energy*, 43 (2018) 4682.
43. Uday Pratap Azad, Monika Singh, Sourav Ghosh, Ashish Kumar Singh, Vellaichamy Ganesan, Akhilesh Kumar Singh & Rajiv Prakash, *Int. J. Hydrogen Energy*, 43 (2018) 20671.
44. Cipriano B. Gozzo, Mario R. S. Soares, Júlio C. Sczancoski, Içamira C. Nogueira & Edson R. Leite, *Int. J. Hydrogen Energy*, 39 (2019) 21659.
45. T. Nagai, N. Fujiwara, M. Asahi, Shin-ichi Yamazaki, Z. Siroma, T. Ioroi, *J. Asian Ceramic Society*, 2 (2014) 329.
46. N. Fradette, B. Marsan, *J. Electrochem. Soc*., 145 (1998) 2320.
47. PH. Vermeiren, R. Leysen, H. W. King, G. J. Murphy, H. Vandenborre, *Int. J. Hydrogen Energy*, 12 (1987) 469.
48. R. N. Singh, J. P. Pandey, K. L. Anitha, *Int. J. Hydrogen Energy*, 18 (1993) 467.
49. S. Trasatti, in *Electrochemical Hydrogen Technology*, ed. Wendt H, Elsevier, Amsterdam, 1990, p. 104.
50. F. Svegl, B. Orel, I. Grabec-Svegl, V. Kaucic, *Electrochimica Acta*, 45 (2000) 4359.
51. R. N. Singh, N. K. Singh, J. P. Singh, *Electrochimica Acta*, 47 (2002) 3873.
52. R. N. Singh, M. Hamdani, J.-F. Koenig, G. Poillerat, J. L. Gautier, P. Chartier, *J. Appl. Electrochem*., 20 (1990) 442.
53. Boyoon Shin, Sangwon Choi & Yongsug Tak, *Int. J. Electrochem. Sci*., 11 (2016) 5900.
54. Zejie Zhang, Debi Zhou, Xuewen Wu, Xinjun Bao, Jingjing Liao & Meisheng Wen, *Int. J. Hydrogen Energy*, 44 (2019) 7222.
55. E. Gileadi, *Electrode Kinetics*, (VCH Publishers Inc., New York), 1993 p.151
56. R. N. Singh, J. P. Pandey, N. K. Singh, B. Lal, P. Chartier, J. F. Koenig, *Electrochim. Acta*, 45 (2000) 1911.